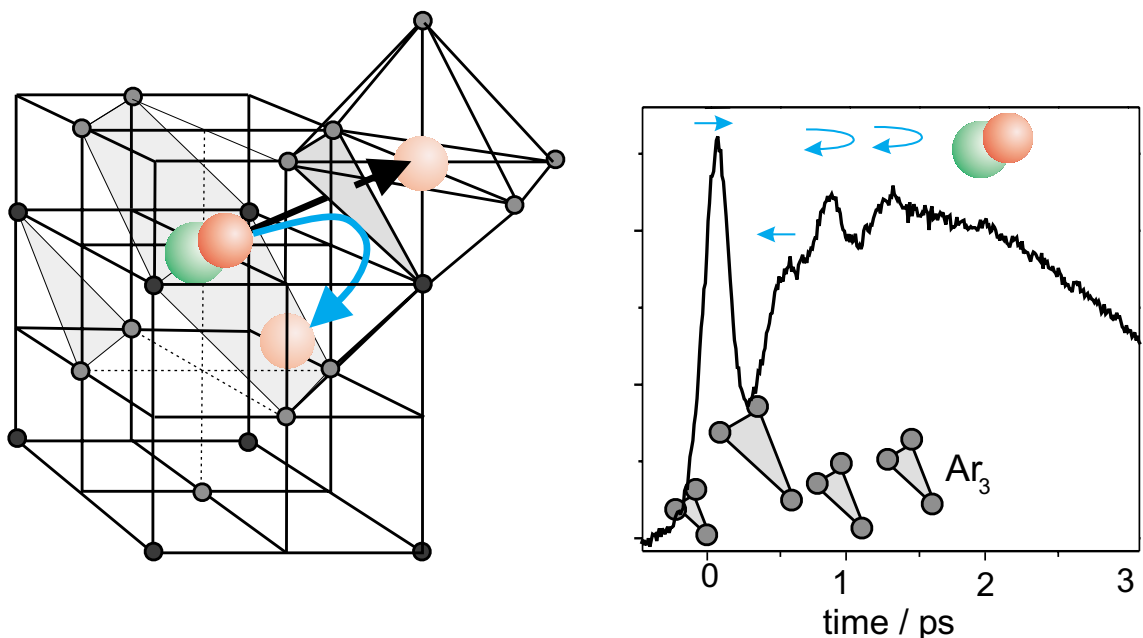


Ultrafast photodynamics in condensed phase: ClF , Cl_2 and I_2 in solid rare gases



Dissertation by
Matias Bargheer
Physics Department
Freie Universität Berlin
2002

Ultraschnelle Photodynamik in kondensierter Phase: ClF , Cl_2 and I_2 in Edelgasfestkörpern

im Fachbereich Physik
der Freien Universität Berlin
eingereichte Dissertation

Matias Bargheer
Mai 2002

Disputationstermin: 17.7. 2002

Erstgutachter: Prof. Dr. N. Schwentner

Zweitgutachter: Prof. Dr. L. Wöste

Abstract

This thesis is part of a project that deals with photochemistry in the condensed phase and is embedded in the collaborative research center "Analysis and Control of Ultrafast Photoinduced Reactions" (SFB 450). Halogens and interhalogens (I_2 , Cl_2 and ClF) in rare gases solids are investigated as model systems by femtosecond-pump-probe spectroscopy.

Coherent wave packet dynamics of I_2 with a period of $T \sim 350$ fs can be observed for more than 10 picoseconds after photoexcitation, despite the strong interactions of the molecule near the dissociation limit with the crystalline Kr matrix. With this system, a novel evaluation scheme for pump-probe spectra is developed and tested, which permits the construction of effective one dimensional potentials of excited electronic states (B and E). An average trajectory of I_2 is measured to visualize the dissipative wave packet dynamics, and vibrational relaxation rates are determined from different signatures of the pump-probe spectra. Near the minimum of the potential, the energy loss is less than 1% per period, but it grows beyond 50% above the gas phase dissociation limit.

The molecules ClF and Cl_2 are examined in Ar and Kr matrices with pump-probe spectroscopy for the first time. The wave packet dynamics of an F fragment that exits the solvent cage is observed in real time. The time for direct cage exit is measured to be $t_{exit} = 250$ fs. Besides the dissociation, the competing recombination of the molecular fragments displays rich dynamics. Above the dissociation limit, the ClF molecule loses more than 35% of its kinetic energy in the first period, whereas the rate slows down to 0.1% near the minimum of the potential. Experimental results evidence a strong coupling of singlet and triplet states, which forces the molecule to recombine into the lowest electronically excited states. Although the spin-orbit coupling of the light atoms Cl and F is weak, the spin-flip occurs in less than $t_f = 500$ fs. Wave packet dynamics persist despite these strong interactions. The scattering of fragments by the cage is compared for molecules with similar electronic states but different isolation geometries in the lattice. A photoselected orientation of the ClF bond in the isotropic Ar cage (single substitutional) is destroyed within $\tau_d = 1.2$ ps, whereas I_2 remains aligned in the fixed cylindrical Kr cage (double substitutional). In co-doped $ClF/Cl_2/Ar$ matrices, the ratio of excited Cl^+Cl^- vs. Cl^+F^- is controlled with a contrast of 1 : 250, using a double-pulse sequence.

The systematic variation of pump and probe wavelength allows for a definite interpretation of the experiments without the aid of calculations, which makes the results particularly valuable for the comparison to the simulations which are simultaneously developed within the SFB 450.

In advance, the spectroscopy of ClF in Ar and Kr was clarified and dissociation yields were measured. Two NOPAs were constructed to provide tunable fs-pulses. The commercial design was improved to double their efficiency. In addition, the implementation of a flexible variant of the FROG technique permits the characterization of the pulse duration and phase of fs-pulses from the IR to the UV.

Kurzfassung

Diese Arbeit ist in einem Projekt entstanden, das sich mit Fragestellungen der Photochemie in der kondensierten Phase beschäftigt und in den Sonderforschungsbereich SFB 450, "Analyse und Steuerung ultraschneller photoinduzierter Reaktionen" eingebettet ist. Als Modellsysteme werden Halogene und Interhalogene (I_2 , Cl_2 und ClF) in Edelgasfestkörpern mit Femtosekunden-Pump-Probe Spektroskopie untersucht.

Trotz der starken Wechselwirkung des I_2 -Moleküls nahe der Dissoziationsgrenze mit der kristallinen Kr -Matrix bleibt eine kohärente Wellenpaketdynamik mit einer Periode von $T \sim 350$ fs über 10 Picosekunden nach der Photoanregung erhalten. Für die Auswertung der Pump-Probe Spektren wird an diesem System ein neues Schema entwickelt und erprobt, das die Konstruktion effektiver eindimensionaler Potentiale von angeregten elektronischen Zuständen (B und E) gestattet. Die dissipative Wellenpaketdynamik des Moleküls wird an einer gemessenen Trajektorie sichtbar gemacht, und verschiedene Signaturen der Ultrakurzzeitspektren dienen der Bestimmung von Schwingungsrelaxationsraten. In der Nähe des Potentialminimums beträgt die Energieabgabe weniger als 1% pro Periode, steigt aber im Bereich der Gasphasendissoziationsgrenze auf Werte über 50% an.

Zum ersten Mal werden die Moleküle ClF und Cl_2 in Ar - und Kr -Matrix mittels Pump-Probe Spektroskopie untersucht. Für ClF in Kr wird die Wellenpaketdynamik beim Austritt eines Fragments (F) aus dem Umgebungskäfig zeitaufgelöst beobachtet. Die gemessene Zeit für den direkten Käfigaustritt beträgt $t_{exit} = 250$ fs. In Konkurrenz zur Dissoziation steht die Rekombination der Molekülfragmente, die eine reichhaltige Dynamik aufweist. Oberhalb der Dissoziationsgrenze verliert ClF über 35% der kinetischen Energie in der ersten Periode, während die Rate im Potentialminimum auf 0,1% pro Schwingung sinkt. Die experimentellen Ergebnisse belegen eine starke nicht-adiabatische Kopplung von Singulett- und Triplettzuständen, die das Molekül sehr schnell in die niedrigsten elektronisch angeregten Zustände relaxieren lässt. Das Umklappen des Spins erfolgt in weniger als $t_f = 500$ fs, obwohl die Spin-Bahn-Kopplung bei leichten Atomen wie Cl und F schwach ist. Trotz dieser starken Wechselwirkungen ist eine Wellenpaketdynamik zu beobachten. Das Streuverhalten der Fragmente am Käfig von geometrisch unterschiedlich eingebauten Molekülen mit ähnlichen elektronischen Zuständen wird verglichen. Wenige Stöße der Fragmente mit dem isotropen Ar -Käfig (einfach substituiert) zerstören eine photoelektivierte Ausrichtung der ClF -Bindung innerhalb von $\tau_d = 1, 2$ ps, während I_2 in seinem zylindrischen Kr -Käfig (zweifach substituiert) starr ausgerichtet bleibt. In gemischt dotierten $Cl_2/ClF/Ar$ -Matrizen lässt sich mit einer Doppelpulsfolge das Verhältnis von angeregtem Cl^+Cl^- gegenüber Cl^+F^- und deren Fluoreszenz mit einem Kontrast von über 1:250 steuern.

Durch systematische Variation der Wellenlängen von Pump- und Probe-Pulsen wird mit den Experimenten eine eindeutige Interpretation erarbeitet, ohne dabei auf Rechnungen zurückzugreifen. Die Ergebnisse sind deshalb besonders geeignet für den Vergleich mit den im SFB 450 parallel laufenden Simulationen.

Die Spektroskopie von ClF in Ar und Kr sowie die Bestimmung der Dissoziationsausbeuten stellen wichtige Vorarbeiten dar. Der Aufbau von zwei neuen NOPAs zur Erzeugung der fs-Pulse resultierte in einer Verdopplung der Effizienz gegenüber dem kommerziellen Gerät. Zudem wurde eine flexible Variante der FROG-Technik implementiert, mit der sich fs-Pulse vom infraroten bis zum ultravioletten Spektralbereich bezüglich ihrer Pulsdauer und Phase charakterisieren lassen.

Contents

| | | |
|----------|--|-----------|
| 1 | Introduction | 1 |
| 2 | Conceptual framework and summary of literature | 5 |
| 2.1 | Simulations of ultrafast dynamics in condensed phase | 5 |
| 2.1.1 | Classical molecular dynamics: I_2/Kr and F_2/Ar | 5 |
| 2.1.2 | Coupling of electronic and nuclear motion | 8 |
| 2.1.3 | DIM and DIIS treatment for potential energy surfaces | 9 |
| 2.1.4 | Non-adiabatic molecular dynamics (DIM - trajectories) | 10 |
| 2.1.5 | Wave packets | 10 |
| 2.2 | Matrix effects and fundamentals | 13 |
| 2.2.1 | The cage effect and isolation of diatomics in solid rare gases | 13 |
| 2.2.2 | Cage exit and isolated F radicals | 14 |
| 2.2.3 | Electronic polarization | 15 |
| 2.2.4 | Nuclear rearrangements | 15 |
| 2.2.5 | Matrix shifts | 18 |
| 2.2.6 | Excimers and exciplexes | 18 |
| 2.2.7 | Molecular ion-pair versus excimer states in condensed rare gas | 19 |
| 2.3 | Femtosecond pump-probe spectroscopy | 20 |
| 2.3.1 | Method | 20 |
| 2.3.2 | The threshold for the probe transition | 22 |
| 2.3.3 | Condensed phase pump-probe spectroscopy | 23 |
| 2.3.4 | Selection rules | 24 |
| 2.3.5 | Polarization dependent pump-probe spectra | 24 |
| 2.3.6 | I_2 in Kr as the model system to advance fs-pump-probe spectroscopy in the condensed phase | 26 |
| 2.4 | The molecule chlorine monofluoride (ClF) | 27 |
| 2.4.1 | Chemical and physical properties | 27 |
| 2.4.2 | Spectroscopy and potential | 27 |
| 2.4.3 | Photochemistry of ClF | 30 |
| 2.4.4 | Stable triatomic rare gas halides in the ground state | 30 |
| 2.4.5 | Electronic states of interhalogens: ClF | 30 |
| 3 | Experimental setup | 33 |
| 3.1 | Ultrahigh vacuum (UHV) setup and cryostat | 33 |
| 3.2 | Sample preparation | 34 |
| 3.3 | Laser system | 35 |
| 3.4 | New NOPA design | 35 |
| 3.4.1 | NOPA setup | 35 |
| 3.4.2 | Adjustment of the main parameters | 37 |

| | | |
|-------|---|----|
| 3.5 | Generation of tunable UV femtosecond pulses | 38 |
| 3.5.1 | Pump pulses at 387 nm | 38 |
| 3.5.2 | Pump and probe pulses from 240 - 360 nm | 39 |
| 3.6 | Pump-probe and FROG setup | 39 |
| 3.7 | Pulse characterization and determination of time zero | 41 |
| 3.8 | Fluorescence detection | 41 |
| 3.9 | Pump-probe setup | 42 |

Part I: Spectroscopy and Photodissociation of ClF in Ar and Kr **44**

| | | |
|----------|--|-----------|
| 4 | Spectroscopic results | 45 |
| 4.1 | Valence states of ClF | 45 |
| 4.1.1 | Absorption | 45 |
| 4.1.2 | Emission from valence states | 45 |
| 4.2 | Ionic states of ClF , Cl_2 and excimers | 48 |
| 4.2.1 | Emission from Cl^+F^- | 48 |
| 4.2.2 | Emission from $Kr_2^+F^-$ exciplex and Cl^+Cl^-/Ar | 49 |
| 4.2.3 | Excited state absorption of ClF and Cl_2 | 53 |
| 4.2.4 | Absorption of KrF | 53 |
| 4.3 | Photobleaching of ClF in Ar and Kr | 54 |
| 4.3.1 | Bleaching of ClF/Ar | 54 |
| 4.3.2 | Bleaching of ClF in Kr | 56 |
| 4.3.3 | Control of dissociation vs. recombination of ClF in Kr | 57 |

| | | |
|----------|--|-----------|
| 5 | Discussion of spectroscopy | 61 |
| 5.1 | Ground and valence states of ClF | 61 |
| 5.1.1 | Emission from valence states of ClF (measure of concentration) | 61 |
| 5.1.2 | Absorption (pump pulse) | 62 |
| 5.2 | Ionic states of ClF , Cl_2 and excimers | 63 |
| 5.2.1 | Emission from ionic states of Cl^+F^- (LIF) | 63 |
| 5.2.2 | Identification of $Kr_2^+F^-$ emission (LIF) | 65 |
| 5.2.3 | Excimer absorption of KrF (probe pulse) | 66 |
| 5.3 | Potential energy surface for ClF in Ar matrix | 68 |
| 5.3.1 | Difference potentials for ClF | 68 |
| 5.3.2 | Difference potential of Cl_2 | 68 |
| 5.4 | Photochemistry of ClF in Ar and Kr | 68 |
| 5.4.1 | Dissociation quantum efficiency | 70 |
| 5.4.2 | Control of F motion: Shuttling F from Cl to Kr | 72 |

Part II: Ultrafast dynamics from pump-probe spectra **74**

| | | |
|----------|--|-----------|
| 6 | Results | 75 |
| 6.1 | Systematic pump-probe spectra on I_2 in Kr | 75 |
| 6.1.1 | Typical B state spectra | 76 |
| 6.1.2 | Polarization analysis of pump-probe spectra | 78 |
| 6.1.3 | A and B'' state spectra | 79 |

| | | |
|---------------------|---|------------|
| 6.2 | Road map for condensed phase pump-probe spectra | 80 |
| 6.3 | Pump-probe spectra for ClF in Ar and Kr | 82 |
| 6.3.1 | B state excitation | 82 |
| 6.3.2 | Polarization dependent pump-probe spectra | 84 |
| 6.3.3 | $^1\Pi$ state excitation | 84 |
| 6.3.4 | Pump-probe spectra with $Kr_2^+F^-$ fluorescence | 87 |
| 6.4 | Pump-probe spectra on Cl_2 in Ar | 89 |
| 6.4.1 | B state excitation | 89 |
| 6.4.2 | $^1\Pi$ state excitation | 92 |
| 7 | Discussion | 93 |
| 7.1 | I_2 in Kr - model data from systematic experiments | 93 |
| 7.1.1 | Vibrational frequencies in the B state | 93 |
| 7.1.2 | Construction of B state potential from pump-probe spectra | 94 |
| 7.1.3 | Construction of E state from pump-probe spectra | 97 |
| 7.2 | Window effects in condensed-phase pump-probe spectra | 98 |
| 7.3 | Wave packet dynamics with strong fragment-cage interaction | 100 |
| 7.3.1 | Construction of an $I - I$ trajectory from pump-probe spectra | 100 |
| 7.3.2 | Recombination dynamics of ClF in Ar | 104 |
| 7.3.3 | Recombination dynamics of Cl_2 in Ar | 107 |
| 7.4 | Vibrational relaxation kinetics of I_2 , ClF and Cl_2 in rare gases | 108 |
| 7.4.1 | Signatures of vibrational relaxation | 108 |
| 7.4.2 | Vibrational relaxation in B state of I_2/Kr from oscillations (method α) | 109 |
| 7.4.3 | Energy dissipation from pump-probe envelope (method β) | 110 |
| 7.5 | Depolarization and angular reorientation | 116 |
| 7.5.1 | Ultrafast reorientation of molecules measured by polarization dependent pump-probe spectroscopy | 116 |
| 7.5.2 | Sterically fixed molecule: I_2/Kr | 118 |
| 7.5.3 | Random scattering in cage: ClF/Ar | 118 |
| 7.6 | Solvent induced spin-flip | 120 |
| 7.6.1 | Spin-flip in F_2 (theory) | 122 |
| 7.6.2 | Spin-flip in ClF (experiment) | 123 |
| 7.6.3 | Comparison of experiment and theory | 125 |
| 7.6.4 | Comparison to I_2 and Cl_2 | 126 |
| 7.7 | Cage exit dynamics of ClF in Kr | 127 |
| 7.7.1 | Direct versus delayed exit | 127 |
| 7.7.2 | Two ultrafast pathways to $Kr_2^+F^-$ | 128 |
| 7.7.3 | Vibration of the Kr cage around F fragments | 129 |
| 7.8 | Relaxation-time-control of Cl_2 vs. ClF | 130 |
| 7.9 | Dissipation and vibrational coherence | 132 |
| 8 | Summary | 133 |
| 9 | Future Prospects | 136 |
| Bibliography | | 137 |
| 10 Appendix | | 151 |

List of Tables

| | | |
|-----|---|-----|
| 2.1 | Ionization potentials and electron affinities | 19 |
| 2.2 | Intensity ratios observed for spectroscopy with polarized light | 26 |
| 4.1 | $A' \rightarrow X$ emission | 49 |
| 5.1 | Potential parameters for ClF in the gas phase and in rare gas matrices | 62 |
| 5.2 | $A' \rightarrow X$ emission | 64 |
| 5.3 | Bond lengths of van-der-Waals RgX molecules and lattice parameters. | 67 |
| 5.4 | Comparison of ClF and F_2 | 71 |
| 7.1 | Spectroscopic parameters T_E | 96 |
| 7.2 | Evaluation of I_2 pump-probe envelope | 111 |
| 7.3 | Evaluation of ClF pump-probe envelope | 113 |
| 7.4 | Vibrational relaxation for ClF/Ar, Cl ₂ /Ar and I ₂ /Kr | 116 |

Abbreviations

Ti:Sa - titanium doped sapphire

SHG - second harmonic generation

(PG)-FROG - (polarization gate)-frequency resolved optical gating

NOPA - non-collinear optical parametric amplifier

LIF - laser induced fluorescence

CARS - Coherent anti-Stokes Raman scattering

DIM - diatomics in molecules

DIIS - diatomics in ionic systems

CI - configuration interaction

MD - molecular dynamics

PES - potential energy surface

RKR - Rydberg-Klein-Rees

fs - femtosecond ($10^{-15}s$)

ps - picosecond ($10^{-12}s$)

a_0 - Bohr radius 5.292×10^{-11} m

List of Figures

| | | |
|------|---|----|
| 2.1 | Classical trajectory calculations for I_2 in Kr | 6 |
| 2.2 | Total energy of I_2 from classical trajectory calculations in Kr | 7 |
| 2.3 | Classical trajectory calculations for F_2/Ar | 8 |
| 2.4 | Tilting of the $F - F$ bond in a recombinig $F - F$ trajectory | 9 |
| 2.5 | ClF and I_2 in fcc rare gas lattice | 13 |
| 2.6 | Potential surface for I_2/Kr from additive pair potentials | 16 |
| 2.7 | Configuration coordinate model | 17 |
| 2.8 | Scheme of pump-probe spectroscopy | 20 |
| 2.9 | Detailed scheme of pump-probe spectroscopy | 21 |
| 2.10 | Distributions of the molecular ensemble after photoselection | 25 |
| 2.11 | Potential of ClF | 28 |
| 2.12 | Absorptions of ClF , Cl_2 , F_2 and ClF_3 Kommentar kommt noch | 29 |
| 2.13 | Orbital diagram of ClF | 31 |
| 2.14 | Orientation of p-orbitals after dissociation | 32 |
| 3.1 | UHV chamber | 34 |
| 3.2 | Block diagram of the laser system | 36 |
| 3.3 | New design of NOPA | 37 |
| 3.4 | Phasematching angle Θ in a NOPA | 38 |
| 3.5 | Pump-probe & FROG setup | 40 |
| 4.1 | Potential diagram of ClF with fluorescences | 46 |
| 4.2 | Vibrational progression of the $A' \rightarrow X$ fluorescence of ClF/Ar | 47 |
| 4.3 | Fluorescence lifetime of $A' \rightarrow X$ | 47 |
| 4.4 | Vibrational progression of the $A' \rightarrow X$ fluorescence of ClF/Kr | 48 |
| 4.5 | $D' \rightarrow A'$ fluorescence of ClF/Ar | 50 |
| 4.6 | $Kr_2^+F^-$ emission | 51 |
| 4.7 | Temperature dependence of $Kr_2^+F^-$ emission | 51 |
| 4.8 | Fluorescence from Cl^+Cl^-/Ar and $Ar_2^+F^-/Ar$ | 52 |
| 4.9 | KrF absorption and excitation spectra | 54 |
| 4.10 | Bleching of the A' emission of ClF/Ar | 55 |
| 4.11 | Bleching of the A' emission of ClF/Ar for different concentrations | 55 |
| 4.12 | Bleching of the A' emission of ClF/Kr | 56 |
| 4.13 | Scheme for control of ClF vs. KrF | 57 |
| 4.14 | Control of dissociation vs. recombination of ClF in Kr | 58 |
| 5.1 | Birge-Sponer plot for the $A' \rightarrow X$ transition of ClF in Ar and Kr | 61 |
| 5.2 | Calculated absorption bands of ClF | 63 |
| 5.3 | Assignment of $Kr_2^+F^-$ emission | 65 |
| 5.4 | $Kr_2^+F^-$ emission compared to literature | 66 |
| 5.5 | KrF potential | 67 |
| 5.6 | Difference potential for ClF | 69 |
| 5.7 | Potential and difference potential for Cl_2 | 70 |

| | | |
|------|--|-----|
| 6.1 | Potential diagram for I_2/Kr | 75 |
| 6.2 | Pump-probe spectra of I_2/Kr | 76 |
| 6.3 | Systematic pump-probe spectra demonstrating the inward/outward splitting | 77 |
| 6.4 | Pump-probe spectra of I_2/Kr on ps timescale | 78 |
| 6.5 | Polarization dependent pump-probe spectrum for I_2/Kr | 79 |
| 6.6 | Excitation of I_2/Kr to states corresponding to spin-flip dynamics in ClF | 80 |
| 6.7 | Guide to pump-probe spectra of diatomics in condensed phase | 81 |
| 6.8 | Pump-probe spectra of ClF/Ar | 83 |
| 6.9 | Oscillations in pump-probe spectra of ClF/Ar | 85 |
| 6.10 | Polarization dependent pump-probe spectrum for ClF/Ar | 86 |
| 6.11 | Pump-probe spectra for different probe wavelengths demonstrating ultrafast spin-flip in ClF/Ar | 86 |
| 6.12 | Pump-probe spectra with on ClF/Kr for different probe wavelengths | 87 |
| 6.13 | Pump-probe spectra with LIF from $Kr_2^+F^-$ at different temperatures | 88 |
| 6.14 | Wave packets of F/Kr | 89 |
| 6.15 | Pump-probe spectra of Cl_2/Ar | 90 |
| 6.16 | Wave packets of Cl_2/Ar | 91 |
| 6.17 | $^1\Pi$ excitation of Cl_2/Ar showing spin-flip | 92 |
| 7.1 | Round-trip times and frequencies of I_2/Kr | 94 |
| 7.2 | Potential energy surface of I_2/Kr constructed from pump-probe spectra | 95 |
| 7.3 | Window effects in pump-probe spectra of I_2/Kr | 98 |
| 7.4 | Connection of the spectral shape of pump and probe pulses with the potential energy surfaces | 99 |
| 7.5 | Trajectory of I_2 with inelastic fragment-cage collision | 101 |
| 7.6 | Sketch of potential and kinetic energy of I_2/Kr and the relevant modes | 102 |
| 7.7 | Potential surfaces of I_2 from DIM trajectory simulations | 103 |
| 7.8 | Wave packet dynamics of ClF/Ar | 105 |
| 7.9 | 2-D potential energy surface of F_2/Ar | 106 |
| 7.10 | 2-D wave packets of F_2/Ar | 107 |
| 7.11 | Energy relaxation rates for I_2/Kr | 110 |
| 7.12 | Energy dissipation in I_2/Kr from pump-probe envelope and oscillations | 111 |
| 7.13 | Comparison of energy relaxation of ClF/Ar vs. Cl_2/Ar | 114 |
| 7.14 | Comparison of energy loss of ClF/Ar , Cl_2/Ar and I_2/Kr | 115 |
| 7.15 | Scheme for angular reorientation: ClF/Ar vs. I_2/Kr | 117 |
| 7.16 | Polarization dependent pump-probe spectrum for ClF/Ar | 119 |
| 7.17 | Snapshots of the molecular dynamics of F_2/Ar_{54} | 120 |
| 7.18 | Populations after excitation to the $^1\Pi$ state: spin-flip | 121 |
| 7.19 | DIM-trajectory demonstrating the mechanism of spin-flip | 122 |
| 7.20 | Potential energy scheme for ClF/Ar for spin-flip experiments | 123 |
| 7.21 | Pump-probe spectra demonstrating ultrafast spin-flip in ClF/Ar | 125 |
| 7.22 | Dissociation and cage exit | 127 |
| 7.23 | Delayed vs. direct cage exit in DIM trajectories | 128 |
| 7.24 | Pump-probe spectrum demonstrating cage exit of F in Kr | 129 |
| 7.25 | Control of Cl^+Cl^- vs. Cl^+F^- population | 130 |